Pore Network Model for Catalytic Dehydration of Methanol at Particle Level

Hossein Beigi, Mitra Dadvar, and Rouein Halladj
Dept. of Chemical Engineering, Center of Excellency for Petrochemical Engineering, Amirkabir University of Technology, Tehran, Iran

DOI 10.1002/aic.11665
Published online December 24, 2008 in Wiley InterScience (www.interscience.wiley.com).

γ-Alumina is used as a catalyst for converting methanol to dimethyl ether. The process takes place in a packed or fluidized bed reactor consisting of microporous particles with distributed pore sizes and interconnectivities. The efficiency of the process is, however, significantly affected by the pore space structure of the particles. All the previous attempts for modeling this phenomenon have used continuum formulation of the problem based on classical equations of mass transport and reaction, without any regards for the effect of pore space morphology. In this article, we study the catalyst's performance by developing a network model for the pore space, with distributed pore sizes and interconnectivities. The network model is used to study the effect of several parameters such as pore space morphology, concentration, and temperature on catalyst's effectiveness factor. The results will be used for reactor simulations. © 2008 American Institute of Chemical Engineers *AIChE J,* 55: 442–449, 2009
Keywords: dimethyl ether, catalyst, diffusion, nonlinear reaction, pore network, effectiveness factor

Introduction

Dimethyl ether (DME) as a clean alternate fuel and as a substitute for chlorofluorocarbons has received growing attention due to environmental pollution and energy consumption. Its physical properties are similar to those of liquefied petroleum gas (LPG) and it is considered as a substitute for diesel fuel. DME does not have carbon–carbon bonds that prevent particulate formation. It is used as a fuel for diesel engines. Furthermore, less carbon monoxide and nitrogen oxides are formed.[1]

DME is traditionally produced by dehydration of methanol which is produced from syngas, products of natural gas reforming.[2] However, in recent years, in some petrochemical plants, it is desired to produce DME from methanol directly.

Different kinds of solid-acid porous catalysts were investigated, Woodhouse[3] and Brake[4] patented that the dehydration of methanol takes place on pure γ-alumina and on modified γ-alumina with phosphates or titans. The performance of modified γ-alumina with silica was investigated by Jun et al.[5] Zeolites were also tested as substitute for γ-alumina.[6,7]

The kinetics of methanol dehydration on acid catalyst has been studied extensively, resulting in different kinetic equations, Bercic and Levec[8] reviewed this kinetics. Most of the kinetic models have derived from the experiments conducted in conditions not found in an industrial reactor. Bercic and Levec[8] reported an intrinsic rate equation which represents the kinetic behavior of the dehydration reaction on γ-alumina more realistically than equations published earlier.

There is already a considerable literature dealing with the problem of designing, modeling, and simulation of DME synthesis reactor. Bercic and Levec[9] compared the experimental data of a packed bed reactor with a one-dimensional plug flow model for an adiabatic fixed bed reactor. They considered catalyst particle as a rigid one and solved continuum diffusion-reaction equation in the particle along with considering temperature changes due to the exothermic reaction to find the effectiveness factor for the catalyst particle.

Correspondence concerning this article should be addressed to M. Dadvar at dadvar@aut.ac.ir.

© 2008 American Institute of Chemical Engineers

Then they used continuum models to predict the plug flow heterogeneous reactor performance by considering fluid flow and reaction terms in the mass transport equation, and heat conduction and heat of the reaction in the energy balance equation. Lu et al.[10] proposed that fluidized bed reactor is an ideal reactor for the highly exothermic DME reaction. Lee et al.[11] simulated a fixed bed reactor for DME synthesis from syngas in a shell and tube-type fixed bed reactor.

All the models that have been developed so far for predicting the performance of the catalyst particle and reactor during DME production from methanol have used continuum equations of mass transport and reaction without any regards for the details of the heterogeneous morphology of the microporous particles. Continuum models can only be applied to a single pore and it is not clear how the results can be extended to porous media that are basically random networks of interconnected pores. They cannot predict the dependence of transport phenomena on the morphology of pore space in catalyst particles; however, pore network modeling can provide such information. Therefore, an accurate description of the phenomena must consider the effect of pore space structure of the particle, which strongly influences the mass transport and reaction in it. The effect of connectivity of a pore space can be represented by the percolation theory that its application to porous media problems was described by Sahimi et al.[12–14] The morphology of the micro porous particle's pore space also has a controlling effect on transport phenomena through pore size distribution. If the pore size distribution is broad, meaning that the pore space consists of very small and very large pores, the transport paths are very tortuous and the small pores control diffusion of the reactants within the pore space. In this condition, there can still be a diffusion limitation effect, even if the flow paths are connected.

To study the effect of the heterogeneities at the micro porous particle level, the pore space can be represented by a network of interconnected bonds and sites. In the catalyst particle, the bonds indicate the pore throats where mass transport and reaction take place, and sites are the places where the pore throats meet and branch out.

The aim of this article is as follows. First, we describe the network model of the particles that we used in this article. Then we present the details of the mass transport and reaction equations within the pores. The results of the computer simulations are then presented and discussed in the following section. After that a summary of the article is given where we will also discuss how we will use the results of the article for reactor modeling.

Network Model of the Pore Space

Any porous medium can, generally, be conformed into an equivalent network of bonds (pore throats) and sites (pore bodies). We refer to bonds and sites as pores and nodes, respectively. We represent the porous catalyst by a three-dimensional simple cubic network with a coordination number $Z = 6$, which is the number of pores that are connected to each other at each node. To study the effect of the connectively, we also generate networks with an average coordination number $<Z>$ other than six. This is accomplished by randomly selecting a fraction p of the bonds

$$p = 1 - \frac{<Z>}{Z}, \tag{1}$$

and removing them from the network.

Table 1. The Parameters Used in Simulations

Properties	Value
Average pore radius r_a*	3.375 (nm)
Specific surface area a*	333.8×10^3 (m^2/kg)
k_s†	$5.35 \times 10^{13} \exp\left(\frac{-17,280}{T}\right)$ (kmol/kgh)
K_M†	$5.39 \times 10^{-4} \exp\left(\frac{8487}{T}\right)$ (m^3/kmol)
K_W†	$8.47 \times 10^{-2} \exp\left(\frac{5070}{T}\right)$ (m^3/kmol)
K†	$0.11 \exp\left(\frac{2712.9}{T}\right)$

*Yaripour et al.[15]
†Bercic and Levec.[8]

The pores are assumed to be cylindrical and the effective radii of them are distributed according to the probability density function (PDF) $f(r)$. In this article, we use the following form for $f(r)$

$$f(r) = \frac{r - r_m}{(r_a - r_m)^2} \exp\left[-\frac{1}{2}\left(\frac{r - r_m}{r_a - r_m}\right)^2\right], \tag{2}$$

where r_a and r_m are the average and minimum pore radius, respectively. The pore size distribution (PSD) $f(r)$ can be measured by a number of methods (e.g., Ref. 14), but usually only the average pore size of the particles is reported. We use a typical value of r_a reported in the literature, which is listed in Table 1. We also vary r_a as one parameter of the simulation to study its effect on the transport phenomena.

We assumed $r_m = r_a/14$. Figure 1 shows the different PSDs used in our simulations. The pores are assumed to have the same length l. The pore's length can be selected from a PDF $g(l)$, but in the absence of any experimental data we fix l. In the following simulations, we assumed $l/r_a \sim 10$. It should be remarked that any kind of network structure can be used to represent the pore space of the catalyst, such as those having different coordination number in the sites of the network. However, it has been shown that if the average coordination number of a random network and that of regular network are equal,[16,17] the transport and reaction in such networks are completely similar. We also tested the sensitivity of the results to the topological properties of the network. In addition if the molecular radii of the reactant or products R_{Mol} are greater than a pore radius, they can not diffuse in that pore. Therefore, the fraction of pores

$$p_M = \int_{r_m}^{R_{Mol}} f(r)\, dr, \tag{3}$$

is too small to permit the molecules pass through them. Thus the molecular size of the components and the pore size structure can also increase diffusion limitation.

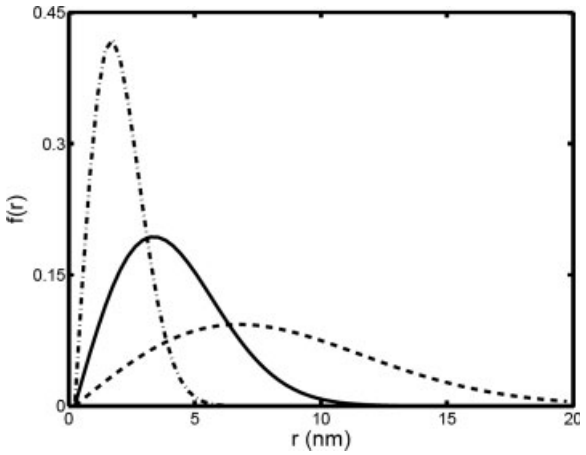

Figure 1. Three pore size distributions used in the simulations, solid curve corresponds to a distribution with an average pore size r_a listed in Table 1, whereas dashed and dashed-doted curves represent 2 r_a and 1/2 r_a.

Diffusion and Reaction Within the Pores

We first discuss the reaction kinetics of the catalytic dehydration of methanol to DME.

$$2(CH_3OH) \Leftrightarrow CH_3OCH_3 + H_2O, \tag{4}$$

The synthesis reaction is catalyzed by the γ-alumina catalyst, Bercic and Levec[8] showed that the rate equation can be considered by the following formula:

$$-r_M = k_s \frac{K_M^2 \left(c_M^2 - \frac{c_D c_W}{K}\right)}{\left(1 + 2\sqrt{K_M c_M + K_W c_W}\right)^4}, \tag{5}$$

where c is concentration and subscripts M, W, and D represent methanol, water, and DME, respectively. The kinetic constants k_s, K_M, K_W, and K which follow Arrhenius and the Vant Hoff relation are listed in Table 1 and the reaction is exothermic.

Now we describe the pore level mass transport and reaction phenomena. The pores are typically very small; diffusion is the main mechanism of mass transport in the particle pore space. As we used $l/r_a \sim 10$, the pore length is large enough to allow using the continuum equations of diffusion and reaction at the pore level. We also assume the steady state conditions dominate, because the deactivation of the catalyst is slow and the changes in the structure of the catalyst particle and pore space due to deactivation are not considered here. In addition, as we are interested in the macroscopic mass transport process, only the variation of the components concentration in the pores' axial direction x is significant. Thus we consider a pore of radius r and write the mass balance for a shell of thickness Δx between axial positions x and $x + \Delta x$, we obtain

$$\frac{d^2 c_k}{dx^2} + 2\frac{\upsilon_k}{a\, r\, D_{K,k}} \left(-r_M\right) = 0, \tag{6}$$

where k refers to each of the components, $D_{K,k}$ is the Knudsen diffusivity, a is the surface area per unit weight of the particle, and υ_k is the stoichiometric constant, which is -2 for M and $+1$ for W and D. Using the expression for reaction rate, Eq. 6 can be written as

$$\frac{d^2 c_k}{dx^2} + 2\frac{\upsilon_k k_s}{a\, r\, D_{K,k}} \left(\frac{K_M^2 \left(c_M^2 - \frac{c_D c_W}{K}\right)}{\left(1 + 2\sqrt{K_M c_M + K_W c_W}\right)^4} \right) = 0, \tag{7}$$

We introduce the dimensionless variables, $C_k = c_k/c_s$ and $z = x/l$ where c_s is the concentration at the catalyst surface, so that at the inlet C_k is the same as mole fraction, and l is the pore length. After simplification we obtain

$$\frac{d^2 C_k}{dz^2} - \upsilon_k\, \varphi_k^2 \left(-R_M\right) = 0, \tag{8}$$

where φ_k is pore level Thiele modulus and $-R_M$ is the dimensionless form of the reaction rate.

$$\varphi_k = \sqrt{\frac{2\, k_s\, l^2}{c_s\, a\, r\, D_{K,k}}},$$
$$-R_M = \frac{K_M^2\, c_s^2 \left(C_M^2 - \frac{C_D C_W}{K}\right)}{\left(1 + 2\sqrt{K_M c_s C_M} + K_W c_s C_W\right)^4}, \tag{9}$$

As the reaction takes place in gas phase, the Knudsen diffusion coefficient for each component is calculated by the following formula[18]:

$$D_{K,k} = \frac{2r}{3}\sqrt{\frac{8RT}{\pi M_k}}, \tag{10}$$

where R is the universal gas constant, T is temperature, and M_k is the molecular weight of component k. It should be remarked that a restricted diffusion mechanism is dominant when diffusing molecules have the same order of magnitude size as catalyst's pores, this is calculated using the following equation[19]

$$D_k = D_{K,k}\left(1 - \frac{R_{Mol}}{r}\right)^4 \tag{11}$$

Considering this mechanism, $D_{K,k}$ has to be replaced by D_k in Eq. 9 for φ_k. We write Eq. 8 for each of the components

$$\frac{d^2 C_M}{dz^2} - 2\,\varphi_M^2 \left(-R_M\right) = 0, \tag{12}$$

$$\frac{d^2 C_D}{dz^2} + \varphi_D^2 \left(-R_M\right) = 0, \tag{13}$$

$$\frac{d^2 C_W}{dz^2} + \varphi_W^2 \left(-R_M\right) = 0, \tag{14}$$

Equations 12–14 are nonlinear diffusion-reaction equations which must be solved subject to the following boundary conditions:

$$C_k(z=0) = C_{k,z0}, \quad C_k(z=1) = C_{k,z1}, \tag{15}$$

As these equations are nonlinear and have no analytical solution, numerical methods must be used to solve them. They have to be solved simultaneously to find the concentration gradient for each of the components in the network. We do not know the concentration of each component at the nodes ($C_{k,z0}$, $C_{k,z1}$). To find them we have to write the mass balance for the components at all the nodes of the network. We assume that no adsorption or chemical reaction takes place at the nodes of the network. If so, the total mass flow of each component that enters a node must be equal to that which leaves the node. Therefore for any node i which is in the network's interior we must have

$$\sum_{\{ij\}} J_{ij} S_{ij} = 0, \tag{16}$$

where J_{ij} is the flux of the components in pore ij and should be considered for each k component separately, $S_{ij} = \pi r_{ij}^2$ is pore ij cross-sectional area, and the sum is over all the pores ij that are connected to site i. The flux J_{ij} is given by

$$J_{ij} = -D_k \left(\frac{c_s}{l}\right) \frac{dC_k}{dz}, \tag{17}$$

where $\frac{dC_k}{dz}$ is the dimensionless concentration gradient of component k in each pore ij that is connected to node i. Equation 16 has to be written for all the nodes in the network (except for the boundary nodes with known concentration). By solving these equations simultaneously in the network, one can find C_k at each node.

The diffusion-reaction Eqs. 12–14 along the pores are nonlinear differential equations with boundary condition of type boundary value problem and one of the best methods for solving them is orthogonal collocation method.[20]

We used this method considering four collocation points along each pore. The collocation points lie on $z = 0$, 0.2113, 0.7887, 1 that we call them Points 1 to 4, respectively. Points 1 and 4 are at the pores' end, which coincide with the nodes to which the pore is connected, and the two other points are along the pores. According to the orthogonal collocation method and the diffusion-reaction equations in each pore, the concentrations at Points 2 and 3 are related to the concentrations at Points 1 and 4, as follows:

$$B_{2,1}C_{k,1} + B_{2,2}C_{k,2} + B_{2,3}C_{k,3} + B_{2,4}C_{k,4} + \upsilon_k \varphi_k^2(-R_{M,2}) = 0, \tag{18}$$

$$B_{3,1}C_{k,1} + B_{3,2}C_{k,2} + B_{3,3}C_{k,3} + B_{3,4}C_{k,4} + \upsilon_k \varphi_k^2(-R_{M,3}) = 0, \tag{19}$$

where $B_{i,j}$s are the known elements of coefficient matrix B which relates to second order derivative term in the orthogonal collocation method and are given in Eq. 20, in $C_{k,j}$ the subscript k represents each of the components and j refers to the collocation points and $-R_{M,2}$, $-R_{M,3}$ are the same as $-R_M$ in Eq. 9 representing the reaction rate at Points 2 and 3.

$$B = \begin{bmatrix} 24 & -37.18 & 25.18 & -12 \\ 16.39 & -24 & 12 & -4.392 \\ -4.392 & 12 & -24 & 16.39 \\ -12 & 25.18 & -37.18 & 24 \end{bmatrix}, \tag{20}$$

We can also combine Eqs. 18 and 19 to find $C_{k,2}$ and $C_{k,3}$ in terms of $C_{k,1}$ and $C_{k,4}$ therefore after simplification we have:

$$C_{k,2} = [(B_{3,3}B_{2,1} - B_{3,1}B_{2,3})C_{k,1} + (B_{3,3}B_{2,4} - B_{3,4}B_{2,3})C_{k,4} + B_{3,3}\upsilon_k \varphi_k^2(-R_{M,2}) - B_{2,3}\upsilon_k \varphi_k^2(-R_{M,3})] \div [B_{3,2}B_{2,3} - B_{2,2}B_{3,3}], \tag{21}$$

$$C_{k,3} = [(B_{3,2}B_{2,1} - B_{3,1}B_{2,2})C_{k,1} + (B_{3,2}B_{2,4} - B_{3,4}B_{2,2})C_{k,4} + B_{3,2}\upsilon_k \varphi_k^2(-R_{M,2}) - B_{2,2}\upsilon_k \varphi_k^2(-R_{M,3})] \div [B_{3,3}B_{2,2} - B_{3,2}B_{2,3}], \tag{22}$$

Therefore, the concentration of each component at Points 2 and 3 in a pore can be found in terms of the concentrations at the nodes connected to that pore and the rate of the reaction at Points 2 and 3.

It should be pointed out that in the simulations here, we did not consider temperature changes due to the exothermic reaction and an isotherm condition is assumed. However, we studied the effect of temperature changes on the catalyst performance.

Monte Carlo Simulation

The simulations are carried out according to the following procedure:

(1) The pore network with the given pore size distribution and finite connectivity is generated.

(2) The boundary conditions that are imposed to the network are specified. In the direction of macroscopic transport, we specify the concentration at the inlet $x = 0$, while a zero flux boundary condition is imposed at $x = L/2$, where L is the pore network length. This boundary condition indicates the symmetry that almost exists in the particle. We used periodic boundary condition in the transverse directions.

(3) To find the concentration distribution of the components in the network, we write Eq. 16 for every interior node of the network and for each of the elements. As the reaction is nonlinear we cannot find $\frac{dC_k}{dz}$ in the flux term which is given by Eq. 17 precisely, therefore it is approximated as

$$J_{ij} = -D_{K,k} \left(\frac{c_s}{l}\right) \frac{\Delta C_k}{\Delta z}, \tag{23}$$

where ΔC_k is the difference between the dimensionless concentrations at each node and its adjacent collocation point in each pore and Δz is the dimensionless distance of them. The concentration at the collocation points is represented by Eqs. 21 and 22 in terms of the node's concentration. Therefore, a set of nonlinear equations is formed in which the nodes' concentrations are unknown.

A trial and error method is used to solve the set of nonlinear equations. As an initial guess, we assumed the concentration of the components at each node and found the concentration of each component at collocation points through Eqs. 18 and 19. The results are only used to calculate the reaction rate $R_{M,2}$ and $R_{M,3}$ at the collocation points as numeric values. Using these values, the set of nonlinear equations is changed to a linear one, which is solved by

conjugate gradient method. The calculated concentration at the nodes was compared with those assumed. The convergence criterion was the difference between two consecutive iterations for concentration of the three components at all the nodes that should be less than 10^{-5}.

(4) The final results are those averaged over eight times realization. To do these simulations we have prepared our own software.

The network must be large enough so that the results are independent of its size. We found that a $40 \times 40 \times 40$ network provides results that are accurate and essentially identical with those obtained with larger networks. The simulations are performed for $20 \times 40 \times 40$ networks, because of the zero boundary condition that we considered at $x = L/2$. In this way, the number of equations will be reduced to half of that of $40 \times 40 \times 40$ networks and the computer runs will be much faster. To do these simulations we have developed our own Fortran program and a Pentium 4 computer (CPU 3 and 256 MB of RAM) is used that takes 2.5 h for computation for each realization.

Before presenting and discussing the results, we should point out that the percolation models of reaction and transport in porous medium were proposed[21,22] and have also been used by several groups.[23–27] The difference between our work and the previous ones is that the reaction kinetics in the present problem is strongly nonlinear which makes the numerical method more complicated and also that we used the orthogonal collocation method to solve diffusion-reaction equations. The other difference is that diffusion-reaction equations were solved simultaneously for three different components to find the concentration distribution in the network.

Results and Discussion

In what follows we will discuss the results of the simulations that we have studied. Figure 2 presents the dimensionless concentration distribution of the components in the particle, while the feed was pure methanol where $L' = L/2$. In this condition, water and DME composition are almost the same. As in the reactor the feed that is in contact with the particles is not always pure, in Figure 3 the feed composition has been varied, so that the dimensionless concentration of methanol at the inlet of the network is considered 0.83 and that of water and DME are equal. In this condition, the composition of water and DME are not the same at the inlet. This figure can be explained through the reaction rate (Eq. 5). According to this equation as water concentration increases, the reaction rate will decrease, therefore a reduction in methanol conversion is observed. It should be also mentioned that the reaction stoichiometery states that the produced moles of DME and water are the same at the end of each pore. Figures 2 and 3 show the average dimensionless concentration of the components in X direction at the discrete nodes in the network not in the pores. Therefore, in spite of different diffusivity coefficient of these components it must not be expected to see various concentration gradients that exist close to each node in these figures. Figure 4 compares the conversion of DME in the particle with the men-

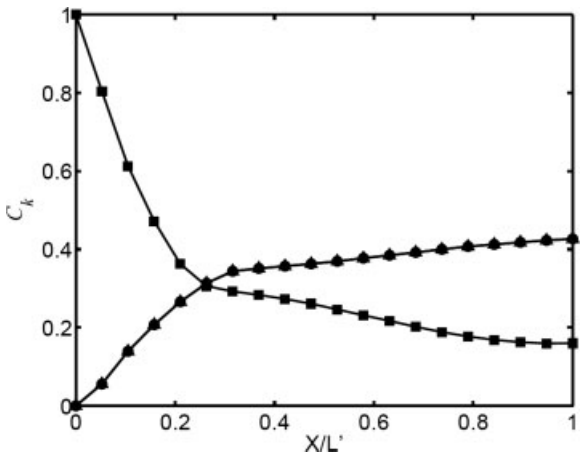

Figure 2. Dimensionless concentration distribution of components in the network while $C_M = 1$ at the inlet, DME (●), water (▲), and (■) methanol.

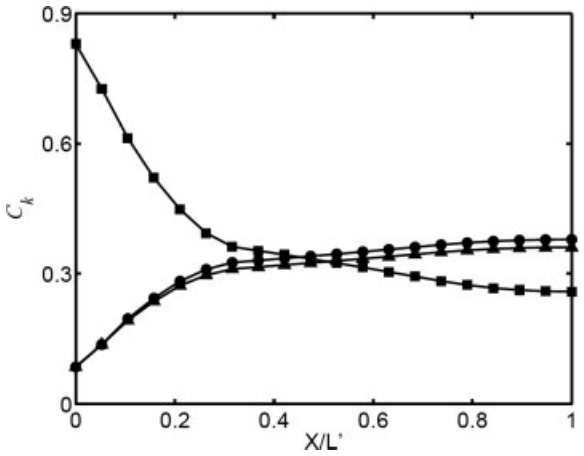

Figure 3. Dimensionless concentration distribution of components in the network while $C_M = 0.83$ at the inlet, DME (●), water (▲), and (■) methanol.

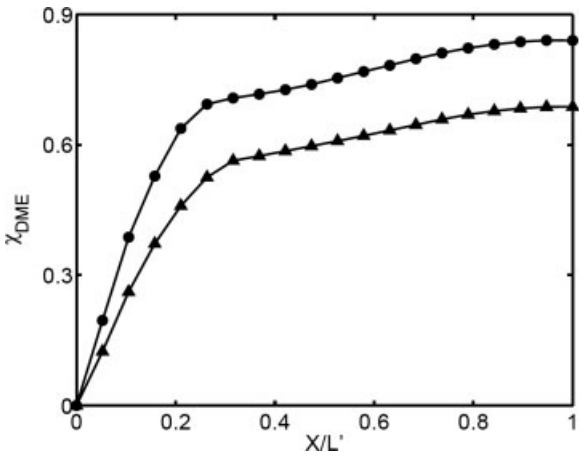

Figure 4. DME conversion in the network for $C_M = 1$ (●) and $C_M = 0.83$ (▲) at the inlet.

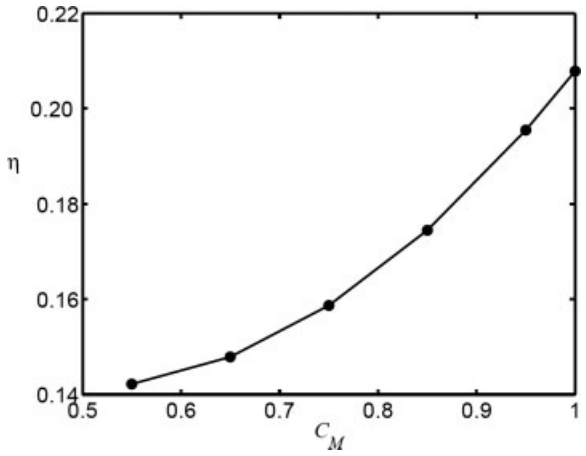

Figure 5. Effectiveness factor vs. methanol mole fraction at the inlet.

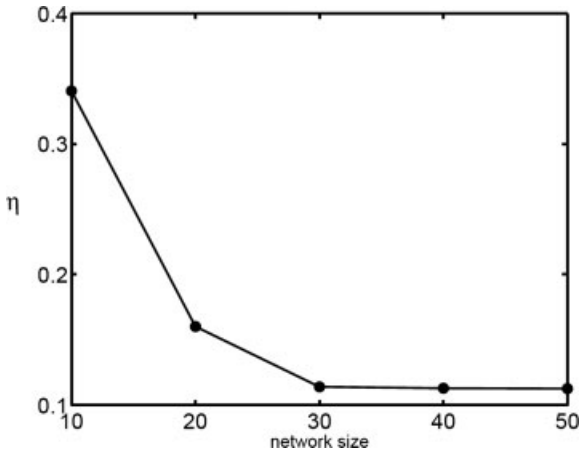

Figure 7. Effectiveness factor vs. network size.

tioned conditions. It is evident that as the inlet mole fraction of methanol decreases, since methanol conversion reduces as well, less conversion of DME would be accessible.

The effectiveness factor η of the pore space vs. the methanol mole fraction at the inlet of the network is shown in Figure 5. In this and other similar figures discussed later, we used the following formula to calculate η

$$\eta = \frac{\sum_{ij} S_{ij} J_{ij}}{\left(\sum_{i=1}^{k} 2\pi r_i l\right) \times \frac{-r_M(c_s, T_s)}{a}} \tag{24}$$

The sum in the numerator is over all pores (with flux J_{ij} and cross-sectional area S_{ij}) that connect the inlet (the left-most face) of the network to its interior, whereas the sum in the denominator is over all the pores in the network having the inlet condition. This is consistent with the classical definition of the effectiveness factor. Figure 5 also indicates that as the water content of the feed is increased, the effectiveness factor is decreased; this result confirms the results of Figure 4 too. Figure 6 presents the dependence of the effectiveness factor on temperature. If the methanol temperature as a pure feed increases, the effectiveness factor is decreased. This is the cause of the dependence of kinetic constants and equilibrium constant of the reaction to temperature. According to Table 1 when the temperature increases these constants decrease and the reaction rate decreases as well. We have also investigated the effect of network size. Figure 7 compares the effectiveness factor for networks of different sizes. It shows that when the network size is large enough the effectiveness factor is independent of the network size. This is why we chose 40 × 40 × 40 networks for the simulations.

The actual pore structure of the catalyst is not a homogeneous one with $Z = 6$. To investigate the effect of the pore space heterogeneities, we have deleted some pores by random to make networks with $<Z>$ other than six, Figure 8 shows the methanol dimensionless concentration distribution in the network for different networks with different percentages of removed pores. As the percentages of the removed

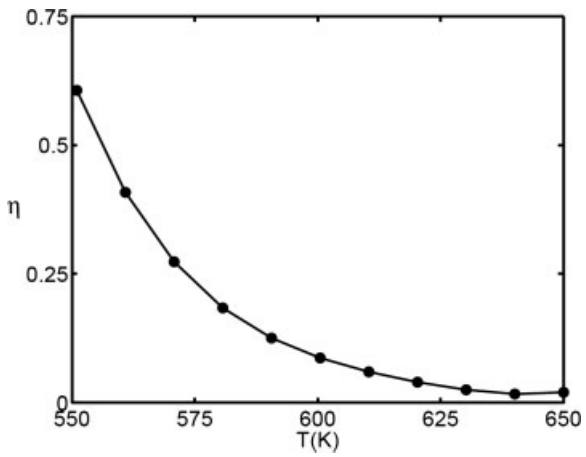

Figure 6. Effectiveness factor vs. temperature while at the inlet $C_M = 1$.

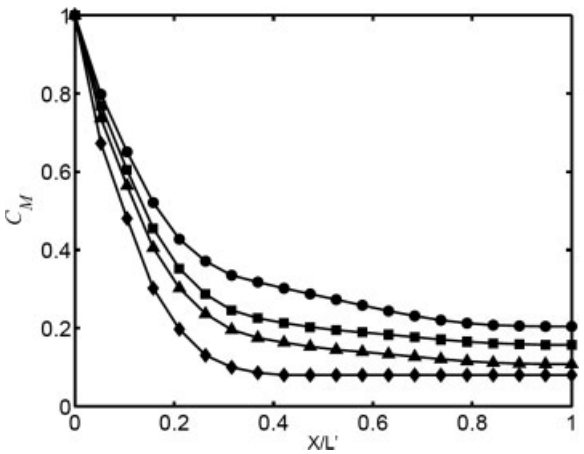

Figure 8. Dimensionless concentration distribution of methanol in the network for different percents of removed pores, p = 0.0% (●), p = 20% (■), p = 40% (▲), and p = 70% (◆).

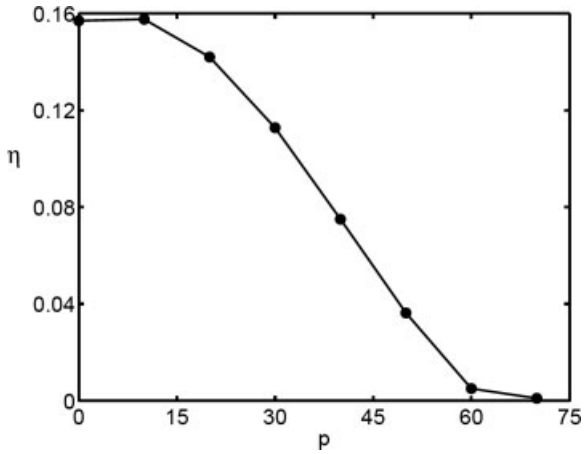

Figure 9. Effectiveness factor vs. percent of removed pores.

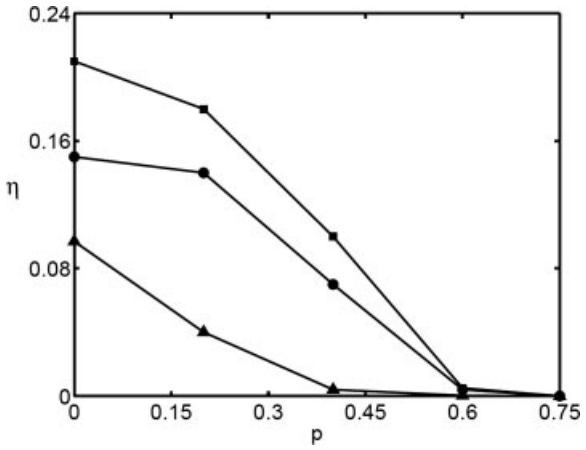

Figure 11. Effectiveness factor vs. fraction of removed pores for different pore size distribution, the base case r_a listed in Table 1 r_a (●), 2 r_a (■), and r_a (▲).

pores in the network increase, the concentration gradient along the network decreases, meaning that the driving force for diffusion in the catalyst is reduced. For removed pores equal to 70%, which is close to percolation threshold in a cubic network, the concentration inside the particle is almost the same. Figure 9 presents the effectiveness factor vs. the percentage of the removed pores. As the connectivity in the network decreases (see Eq. 1) the diffusion limitation gets stronger and the effectiveness factor or performance of the catalyst decreases too. The amount of DME production is presented in Figure 10. This figure also confirms the results of Figures 8 and 9. As the average coordination number in the network decreases, less DME is produced. We also studied the effect of pore size distribution by varying the average pore size r_a (see Eq. 2). The base case was the same as before; we also calculated the effectiveness factor for the cases in which the average pore size was half, and double. Figure 11 presents the effectiveness factor vs. the percentage of removed pores for different PSDs. According to this figure, PSD can strongly affect effectiveness factor and catalyst performance. In this figure the curve related to $r_a/2$ has a different shape comparing with the others. This is because with this PSD the diameter of many pores is less than the component's diameter which causes diffusion and reaction cannot happen in them and they behave as closed pores. The diffusion limitation is stronger at this condition and hindered diffusion is dominant. Figure 12 also shows the amount of DME formation in these networks. This figure also indicates that networks with greater r_a have higher performance. According to this figure, the performance of particles having a more heterogeneous pore structure has also decreased.

These conclusions show that the morphology of the particle greatly influences the performance of the catalyst. These aspects of modeling this phenomena cannot be predicted by any of the past continuum models.

Summary

The results of the pore network simulation presented in this article, indicate the strong effect of pore structure on the

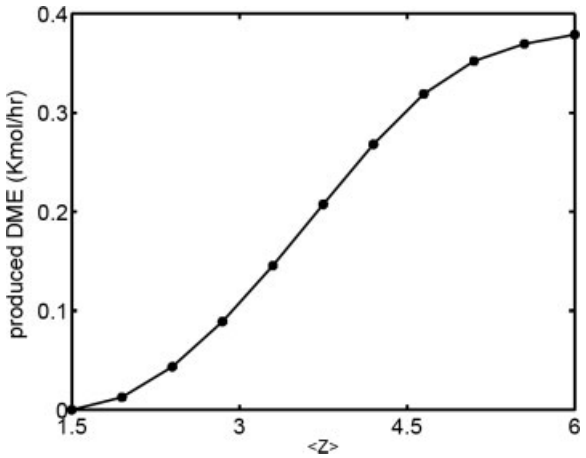

Figure 10. Amount of produced DME vs. average coordination number of the network.

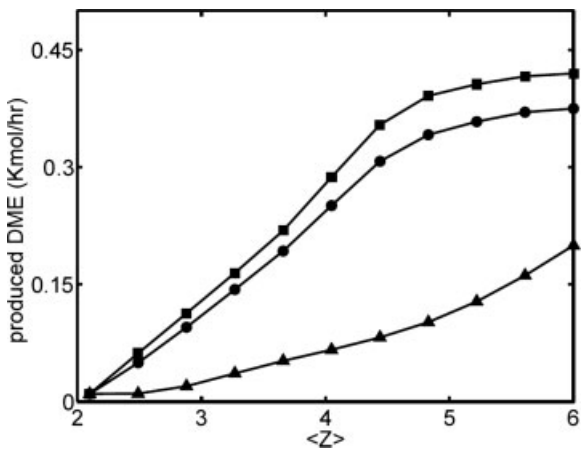

Figure 12. Amount of produced DME vs. average coordination number for different pore size distribution, r_a (●), 2 r_a (■), and r_a (▲).

performance of microporous particles and the diffusion-reaction phenomena which affects the efficiency of conversion of methanol to DME. The effect of this factor is manifested on the methanol and DME concentration profiles, the effectiveness factor of the particles and the amount of DME produced. Moreover, our simulations demonstrate that reasonable modeling for considering the effect of the pore space morphology requires pore network modeling.

The variation of the effectiveness factor with pore space structure, concentrations of input methanol and temperature, which are those shown in Figures 5, 6, 9, and 11 will be used as the input data for the simulation and prediction of methanol conversion and DME formation at the reactor level.

Using appropriate values for the effectiveness factor along the reactor and considering its changes with pore space morphology, concentration, and temperature of the components would help to predict a more realistic performance of the reactor.

Literature Cited

1. Hansen JB, Oishi T. Dimethyl ether (DME) as clean fuel for diesel engines. *Petrotech*. 1997;20:823.
2. Ng KL, Chadwick D, Toseland BA. Kinetics and modeling of dimethyl ether synthesis from synthesis gas. *Chem Eng Sci*. 1999; 54:3587.
3. Woodhouse JC. US Patent. 2,104,408 (1935).
4. Brake LD. Preparation of dimethyl ether by catalytic dehydration of methanol. US Patent. 1986;4:595–785.
5. Jun KW, Lee HS, Roh HS, Park SE. Catalytic dehydration of methanol to dimethylether (DME) over solid-acid catalysts. *Bull Kor Chem Soc*. 2002;23:803.
6. Jiang S, Hwong JS, Jin T, Cho W, Beak YS, Park SE. Dehydration of methanol to dimethyl ether over ZSM-5 Zeolite. *Bull Kor Chem Soc*. 2004;25:185.
7. Kubelkova L, Novakova J, Nedomova K. Reactivity of surface species on zeolites in methanol conversion. *J Catal*. 1990;124:441.
8. Bercic G, Levec J. Intrinsic and golbal reaction rate of methanol dehydration over γ-Al_2 O_3 pellets. *Ind Eng Chem Res*. 1992;31: 1035.
9. Bercic G, Levec J. Catalytic dehydration of methanol to dimethyl ether investigation and reactor simulation. *Ind Eng Chem Res*. 1993;32:2478.
10. Lu WZ, Teng LH, Xiao WD. Simulation and experiment study of dimethyl ether synthesis from syngas in a fluidized-bed reactor. *Chem Eng Sci*. 2004;59:5455.
11. Lee SB, Cho W, Park DK, Yoon ES. Simulation of fixed bed reactor for dimethyl ether synthesis. *Korean J Chem Eng*. 2006;23:522.
12. Sahimi M, Gavalas GR, Tsotsis TT. Statistical and continuum models of fluid-solid reaction in porous media. *Chem Eng Sci*. 1990;45:1443.
13. Sahimi M. *Application of percolation theory*. London: Taylor & Francis, 1994.
14. Sahimi M. *Flow and transport in porous media and fractured rock*. Weinheim, Germany: VCH, 1995.
15. Yaripour F, Baghaei F, Schmidt I, Perregaard J. Catalytic dehydration of methanol to dimethyl ether over solid-acid catalysts. *Catal Commun*. 2005;6:147.
16. Jerauld GR, Scriven LE, Davis HT. Percolation and conduction on the 3D Voronoi and regular networks: a second case study in topological disorder. *J Phys C*. 1984;17:3429.
17. Sahimi M, Tsotis TT. Transient diffusion and conduction in heterogeneous media: Beyond the classical effective-medium approximation. *Ind Eng Chem Res*. 1997;36:3043.
18. Knudsen M. *Kinetic Theory of Gases: Some Modern Aspects*, 3rd Ed, New York: Wiley, 1950.
19. Spry JC Jr, Sawyer WH. Configuraional diffusion effects in catalytic demetallization of petroleum fractions. In the 68th AICHE Annual Meeting, Los Angeles, California, 1975.
20. Finlayson BA. *Nonlinear Analysis in Chemical Engineering*. USA: McGraw-Hill, 1980.
21. Mohanthy KK, Ottino JM, Davis HT. Reaction and transport in disordered media: Introduction of percolation concepts. *Chem Eng Sci*. 1982;37:905.
22. Sahimi M, Tsotsis TT. A percolation model of catalyst deactivation with site coverage and pore blockage. *J Catal*. 1985;96:552.
23. Mann R, Sharatt PN, Thomson G. Deactivation of a supported zeolite catalyst: diffusion, reaction and coke deposition in stochastic pore network. *Chem Eng Sci*. 1986;41:711.
24. Shah N, Ottino JM. Transport and reaction in evolving disordered composites. II. Coke deposition in a catalyst pellet. *Chem Eng Sci*. 1987;42:73.
25. Beyne AOE, Froment GF. A percolation approach for the modeling of deactivation of zeolite catalysts and coke formation. *Chem Eng Sci*. 1990;45:2089.
26. Zhang L, Seaton NA. Simulation of catalyst fouling at the particle and reactor levels. *Chem Eng Sci*. 1996;51:3257.
27. Dadvar M, Sahimi M. Pore network model of deactivation of immobilized glucose isomerase in packed-bed reactors. II. Three-dimensional simulation at the particle level. *Chem Eng Sci*. 2002;57:939.

Manuscript received Nov. 19, 2007, and revision received Aug. 12, 2008.